Author/s:
Song, J;Cortez-Jugo, C;Shirbin, SJ;Lin, Z;Pan, S;Qiao, GG;Caruso, F

Title:
Immobilization and Intracellular Delivery of Structurally Nanoengineered Antimicrobial Peptide Polymers Using Polyphenol-Based Capsules

Date:
2022-02-02

Citation:
Song, J., Cortez-Jugo, C., Shirbin, S. J., Lin, Z., Pan, S., Qiao, G. G. & Caruso, F. (2022). Immobilization and Intracellular Delivery of Structurally Nanoengineered Antimicrobial Peptide Polymers Using Polyphenol-Based Capsules. ADVANCED FUNCTIONAL MATERIALS, 32 (6), https://doi.org/10.1002/adfm.202107341.

Immobilization and Intracellular Delivery of Structurally Nanoengineered Antimicrobial Peptide Polymers Using Polyphenol-Based Capsules

*Jiaying Song, Christina Cortez-Jugo, Steven J. Shirbin, Zhixing Lin, Shuaijun Pan, Greg G. Qiao, and Frank Caruso**

Dr. J. Song, Dr. C. Cortez-Jugo, Dr. Z. Lin, Dr. S. Pan, Prof. F. Caruso
ARC Centre of Excellence in Convergent Bio-Nano Science and Technology, and the Department of Chemical Engineering,
The University of Melbourne, Parkville, Victoria 3010, Australia
E-mail: fcaruso@unimelb.edu.au

Dr. S. J. Shirbin, Prof. G. G. Qiao
Polymer Science Group, the Department of Chemical Engineering
The University of Melbourne, Parkville, Victoria 3010, Australia

Keywords: antimicrobial, intracellular delivery, peptides, star polymers, tannic acid

Structurally nanoengineered antimicrobial peptide polymers (SNAPPs) are an emerging class of antimicrobials against multidrug-resistant bacteria. Their encapsulation in particle carriers can improve their therapeutic efficacy by preventing peptide degradation, reducing clearance, and enhancing intracellular delivery and dosage to bacteria-infected host cells. Herein, two template-mediated strategies are reported for immobilizing SNAPPs in microcapsules through (1) complexation of SNAPPs with tannic acid (TA) onto porous $CaCO_3$ templates and subsequent removal of the templates (SNAPP–TA capsules) and (2) adsorption of SNAPPs onto $CaCO_3$ templates and subsequent encapsulation within a metal–phenolic (Fe^{III}–TA) coating and template removal (SNAPP–Fe^{III}–TA capsules). The loading amounts of SNAPPs are 0.8 and 4.4 pg per SNAPP–TA and SNAPP–Fe^{III}–TA capsule, respectively. At pH 7.4, there is sustained release of SNAPPs, which retain high antimicrobial activity with minimum inhibitory concentration values of ~30 μg mL^{-1} in *Escherichia coli.* Both capsule systems are internalized by alveolar macrophages in vitro, with negligible cytotoxicity and are amenable to nebulization, remaining stable in nebulized droplets. This study demonstrates the potential of engineered polyphenol-based capsules for peptide drug immobilization and intracellular delivery, which have prospective application in the pulmonary delivery of antimicrobials against respiratory bacterial infections (e.g., pneumonia, tuberculosis).

1. Introduction

Bacteria are a common cause of lung infections in the lower respiratory regions.[1] Clinically, the widely used therapy for treating bacterial infection in the lungs is to administer antibiotics via oral, intravenous, or pulmonary routes.[2] However, there is an increasing incidence of antibiotic resistance among bacteria owing to the increased use of antibiotics, leading to reduced therapeutic efficacy.[3] To address the need for improved antibiotics, a class of synthetic antimicrobial peptide mimics termed structurally nanoengineered antimicrobial peptide polymers (SNAPPs) was developed via ring-opening polymerization (ROP) of lysine (Lys) and valine (Val) *N*-carboxyanhydride (NCA) monomers initiated from the terminal amines of a poly(amido amine) (PAMAM) dendrimer core (**Figure 1**a).[4] The SNAPPs exhibit excellent antimicrobial activity in vivo with low toxicity toward mammalian cells and negligible bacterial resistance and thus have been considered to be promising candidates against bacterial infection, including infection in lungs (e.g., tuberculosis and pneumonia).[4–7] Compared with oral or intravenous administration, the delivery of SNAPPs via the pulmonary route could allow a more rapid onset of action and potentially enhance the therapeutic efficacy for the treatment of bacterial lung infections, as the SNAPPs can be delivered to the target lung region directly, thereby avoiding first-pass metabolism and systemic circulation.[8] A conventional approach to pulmonary delivery includes inhalation of a nebulized dry powder or a liquid drug formulation, which requires the drugs to be physicochemically stable during the drying or aerosolization process and the aerodynamic size of the formulations to range between 1 and 5 μm to allow deposition deep in the lungs.[8–10] However, engineering formulations with tailored sizes and properties for precise lung deposition and controlled drug release in target areas is challenging in pulmonary delivery.[11] With advances in nanotechnology, a variety of nanoengineered materials with defined properties and functions, including liposomes,[12] polymersomes,[13] micelles,[14] dendrimers,[15] silica nanoparticles,[16] polymer particles,[17] and polymer capsules,[18] have been developed as drug delivery carriers

that enable improved bioavailability and enhanced delivery efficacy.[19–22] Compared with the conventional delivery of therapeutic formulations, particle-based pulmonary delivery can offer distinct advantages, for example: encapsulation and codelivery of multiple cargos; protection of the encapsulated drugs against deactivation or enzymatic and hydrolytic degradation; controlled drug release over prolonged times; overcoming biological barriers; and targeting to specific structures or cells by manipulating the physicochemical properties (e.g., size, shape, surface chemistry, and mechanical property) of the particles.[23–28]

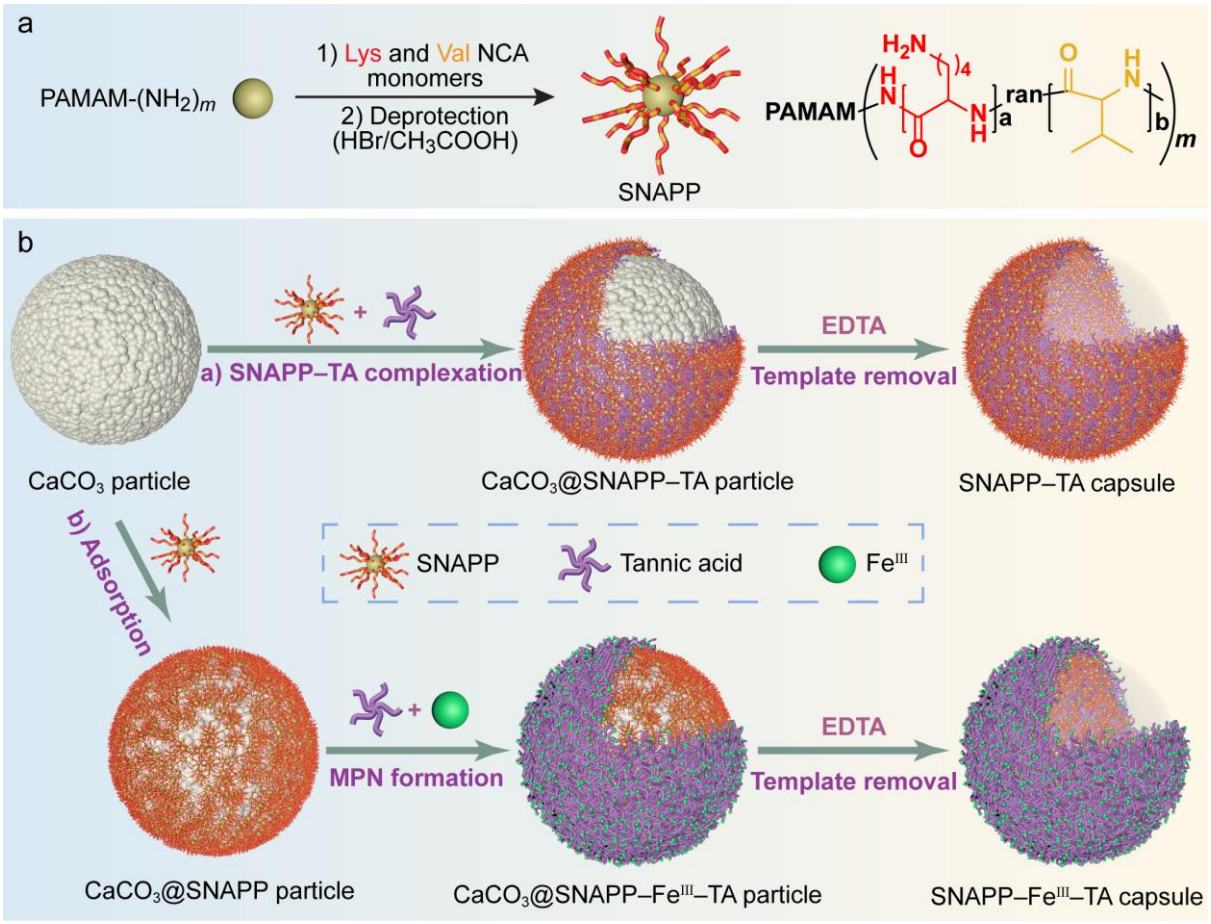

Figure 1. (a) Schematic illustration of the synthesis of SNAPPs via ROP of Lys and Val NCA monomers initiated from the terminal amines of PAMAM dendrimers. (b) Schematic representation of the immobilization of SNAPPs via the assembly of SNAPP–TA or SNAPP–Fe^{III}–TA capsules onto sacrificial $CaCO_3$ particle templates.

Polyphenols, e.g., tannic acid (TA), are naturally occurring compounds widely found in various sources including plants and can form complexes or conjugates with metal ions via coordination bonding or biomacromolecules (e.g., DNA and proteins) via complex

interactions, including electrostatic interactions, hydrogen bonding, and hydrophobic interactions.[29–31] Furthermore, polyphenols have been reported to form multifunctional coatings on various types of substrates of different shapes and compositions via the formation of metal–phenolic networks (MPNs) or protein–phenolic assemblies.[31–36] When assembly is performed on particle templates and the cores (templates) are subsequently removed, polyphenol-based capsules are formed. These capsules are promising carriers for therapeutics owing to their distinct properties, including their versatility in encapsulating a range of therapeutic cargos, their high biocompatibility, and tunable pH-responsiveness and surface properties.[37–40] For example, protein–polyphenol capsules allow immobilization of multiple proteins for different biological applications including enzyme catalysis, fluorescence imaging, and cancer cell targeting.[33] Furthermore, varying the metal ions or phenolic ligands allows the engineering of MPN capsules with specific properties for pH-dependent capsule degradation and drug release,[39] cell targeting,[41] or imaging applications.[32] We recently explored the use of MPN capsules as pulmonary delivery carriers with tunable aerodynamic diameters for controlled lung deposition.[40] Their amenability to nebulization, and in vitro airway distribution, in vivo lung retention, lung cell interaction, biodegradation, inflammatory behavior, and toxicity were assessed.[40] Our study showed that MPN capsules can be delivered to the deep region of the lungs and preferentially associate with alveolar macrophages and neutrophils without causing overt lung inflammation or toxicity, thus demonstrating their potential as drug carriers for pulmonary delivery.[40]

Herein, we report the immobilization of SNAPPs in polyphenol-based capsules and their intracellular delivery in alveolar macrophages. Two methods of SNAPP immobilization are investigated via (i) the assembly of polyphenol-based microcapsules consisting of SNAPPs complexed with TA (denoted as SNAPP–TA capsules) and (ii) the entrapment of SNAPPs within an Fe^{III}–TA metal–phenolic shell (denoted as SNAPP–Fe^{III}–TA capsules) using a

sacrificial calcium carbonate ($CaCO_3$) particle templating method (Figure 1b). The two methods of SNAPP immobilization allow comparison of the loading and release of active SNAPPs from the capsules and their intracellular localization in alveolar macrophages, which are demonstrated in this study. Moreover, it demonstrates the amenability of the peptide-loaded polyphenol-based capsules to nebulization, providing prospects for their potential use as antimicrobials against lung bacterial infections (e.g., tuberculosis, pneumonia) via pulmonary delivery.

2. Results and Discussion

2.1. Synthesis and Characterization of SNAPP–TA and SNAPP–Fe^{III}–TA Capsules

SNAPPs were synthesized following a previously reported method via ROP of cationic Lys and hydrophobic Val NCA monomers initiated by the terminal primary amines of a PAMAM core (Figure 1a).[4] The NCA monomers randomly polymerized to form polypeptide arms with a Lys-to-Val molar ratio of 2:1 (Figure S1). The Lys residues were then deprotected by adding hydrobromic acid (HBr), resulting in water-soluble polymers. Variations in the structure and overall molecular weight of SNAPPs were achieved by using PAMAM dendrimer cores of different generations (generations 0–2, G0–G2) that have a defined number of reactive primary amine initiation sites (Scheme S1). Large SNAPPs (denoted as ^{L}SNAPPs) with a hydrodynamic diameter (D_H) of 10.1 ± 0.5 nm and molecular weight (M_w) of 48.7 kDa, and small SNAPPs (denoted as ^{S}SNAPPs) with a D_H of 2.6 ± 0.1 nm and M_w of 3.3 kDa were synthesized from G2 PAMAM and G0 PAMAM cores, respectively (Scheme S1, Figure S1 and S2). These SNAPPs exhibited similar surface charges in buffers ranging from pH 3.0 to pH 9.0 (8–40 mV) (Figure S3). ^{L}SNAPPs, which are expected to display higher antimicrobial activity than ^{S}SNAPPs,[5] were investigated in detail in this study.

Two methods of SNAPP immobilization were investigated by fabricating SNAPP–TA or SNAPP–Fe^{III}–TA capsules via template-mediated assembly (Figure 1b). Porous $CaCO_3$ particles with an average diameter of 1.8 ± 0.1 μm were prepared as described previously[40,42] and used as sacrificial templates (Figure S4). Based on previous studies, the $CaCO_3$ particles have a crystalline framework with a porous surface structure.[40,42] To fabricate SNAPP–TA capsules, TA and SNAPP solutions were successively added to a suspension of $CaCO_3$ particles and incubated for 6 h, allowing the formation of SNAPP–TA assemblies and their deposition onto the $CaCO_3$ particles. SNAPP–TA capsules were obtained by removal of the $CaCO_3$ templates using ethylenediaminetetraacetic acid (EDTA). To prepare SNAPP–Fe^{III}–TA capsules, SNAPPs were first loaded by adsorption onto $CaCO_3$ particles. After thorough washing to remove excess SNAPPs, iron(III) chloride hexahydrate ($FeCl_3 \cdot 6H_2O$) and TA solutions were sequentially added to the SNAPP-loaded $CaCO_3$ particles followed by the addition of 3-(*N*-morpholino)propanesulfonic acid (MOPS) buffer to raise the pH of the mixture, allowing the assembly of Fe^{III}–TA complexes and the formation of MPNs on the SNAPP-loaded particles. Fe^{III} was used as inhaled MPN capsules containing Fe^{III} have been demonstrated to be non-toxic in vivo.[40] After removal of the $CaCO_3$ templates using EDTA, monodisperse SNAPP–Fe^{III}–TA capsules were obtained. Our previous study has demonstrated the absence of EDTA in TA–Fe^{III} capsules following $CaCO_3$ template removal,[35] and hence EDTA is not expected to affect the functional properties of the capsules.

To enable visualization and characterization of the capsules, fluorescently labeled SNAPPs were used. The characterization of SNAPP–TA and SNAPP–Fe^{III}–TA capsules prepared from fluorescein isothiocyanate (FITC)-labeled ^{L}SNAPPs (denoted as ^{L}SNAPP–TA and ^{L}SNAPP–Fe^{III}–TA capsules, respectively) is shown in **Figure 2**. The differential interference contrast (DIC) microscopy (Figure 2a,f) and fluorescence microscopy (Figure 2b,g) images indicate

that both ^{L}SNAPP–TA and ^{L}SNAPP–Fe^{III}–TA capsules were well dispersed in aqueous solution, showing homogeneous fluorescence and sizes (diameters of 1.9 ± 0.1 μm and 1.8 ± 0.2 μm, respectively) similar to the $CaCO_3$ templates. Transmission electron microscopy (TEM) (Figure 2c,h), scanning electron microscopy (SEM) (Figure 2d,i), and atomic force microscopy (AFM) (Figure 2e,j) images revealed the morphology and structures of the capsules. Both ^{L}SNAPP–TA and ^{L}SNAPP–Fe^{III}–TA capsules appeared collapsed and deformed after air-drying. Furthermore, the ^{L}SNAPP–TA capsules featured typical folds and creases, as consistent with those observed for MPN capsules,[32,39] and they had a shell thickness of 23 ± 2 nm, as measured by AFM (Figure S5a). The ^{L}SNAPP–Fe^{III}–TA capsules exhibited a more rigid structure with a thicker shell (39 ± 7 nm) (Figure S5b) than the ^{L}SNAPP–TA capsules or Fe^{III}–TA films on non-porous substrates (~10 nm).[31] This is likely due to the adsorption of large amounts of SNAPPs on the surface or interior of the porous $CaCO_3$ particles, which might consequently promote the deposition of Fe^{III}–TA complexes onto the particles owing to interactions between SNAPPs and TA. We have previously reported the mechanical properties of Fe^{III}–TA capsules.[31,40] Fe^{III}–TA capsules prepared using porous $CaCO_3$ templates (as in the current study) had thicker shells (108 ± 30 nm) with stiffness of 414 ± 130 mN m^{-1}, as determined by force–deformation measurements using AFM.[40] The use of higher concentrations of $FeCl_3{\cdot}6H_2O$ (4× higher) and TA (8× higher) solutions resulted in thicker ^{L}SNAPP–Fe^{III}–TA capsules (thickness of 269 ± 26 nm), which had a rougher surface and a denser structure, thus showing less collapse and deformation upon air-drying (denoted as ^{L}SNAPP–Fe^{III}–TA (thick) in Figure S5c and S6). As a comparison, the SNAPP–TA and SNAPP–Fe^{III}–TA capsules prepared from ^{S}SNAPPs (denoted as ^{S}SNAPP–TA and ^{S}SNAPP–Fe^{III}–TA capsules, respectively) had similar morphologies and structures to the corresponding capsules prepared from ^{L}SNAPPs (Figure S7), thus demonstrating the versatility of the current immobilization strategies in encapsulating SNAPPs. Proteins immobilized with polyphenols using similar strategies described in this study have previously

been characterized using a host of techniques, including circular dichroism, UV–vis spectroscopy, and gel electrophoresis, to determine parameters, including composition and TA and protein mass ratios.[33,43] Similarly, the basic chemical characterization of TA–Fe^{III} capsules have been performed using energy-dispersive X-ray spectroscopy, Fourier transform infrared spectroscopy, and X-ray photoelectron spectroscopy, as described in the studies therein.[31,32,40]

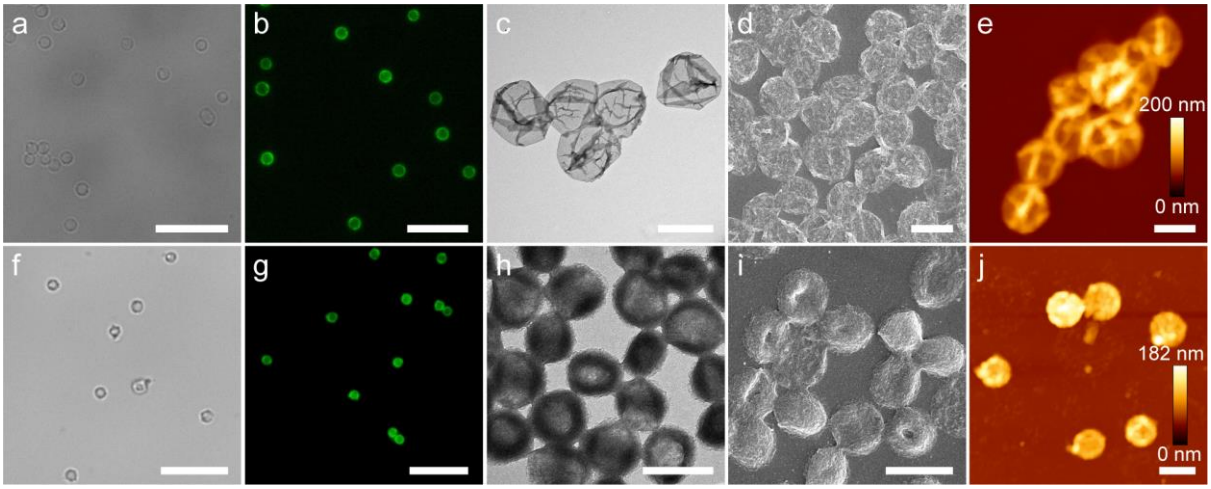

Figure 2. (a, f) DIC microscopy, (b, g) fluorescence microscopy, (c, h) TEM, (d, i) SEM, and (e, j) AFM images of ^{L}SNAPP–TA capsules (a–e) and ^{L}SNAPP–Fe^{III}–TA capsules (f–j), respectively. Scale bars are 10 µm in (a, b, f, g) and 2 µm in (c–e and h–j).

2.2. SNAPP Loading and In Vitro Release

The SNAPP loading capacity of the SNAPP–TA and SNAPP–Fe^{III}–TA capsules was dependent on the SNAPP feed concentration (**Figure 3**a and S8). In general, the SNAPP loading amount increased with increasing SNAPP feed concentration, with a maximum ^{L}SNAPP loading amount of 0.8 pg per capsule for the ^{L}SNAPP–TA capsules and 4.4 pg per capsule for the ^{L}SNAPP–Fe^{III}–TA capsules (Figure 3a); however, the loading efficiency (percentage of the amount of SNAPPs loaded relative to the amount of SNAPPs in the feed solution) decreased with increasing SNAPP concentration (Figure 3b). The ^{L}SNAPP–Fe^{III}–TA capsules immobilized a larger amount of SNAPPs than the ^{L}SNAPP–TA capsules at SNAPP feed concentrations above 0.4 mg mL^{-1}, probably because of the initial SNAPP adsorption/deposition step in the preparation of SNAPP–Fe^{III}–TA capsules that resulted in a

higher loading of the SNAPPs onto the surface and porous interior of the $CaCO_3$ templates. In comparison, SNAPP–TA mostly deposited as complexes on the template surface, as suggested by the thinner shell of the SNAPP–TA capsules compared with the shell thickness of the SNAPP–Fe^{III}–TA capsules (as discussed above).

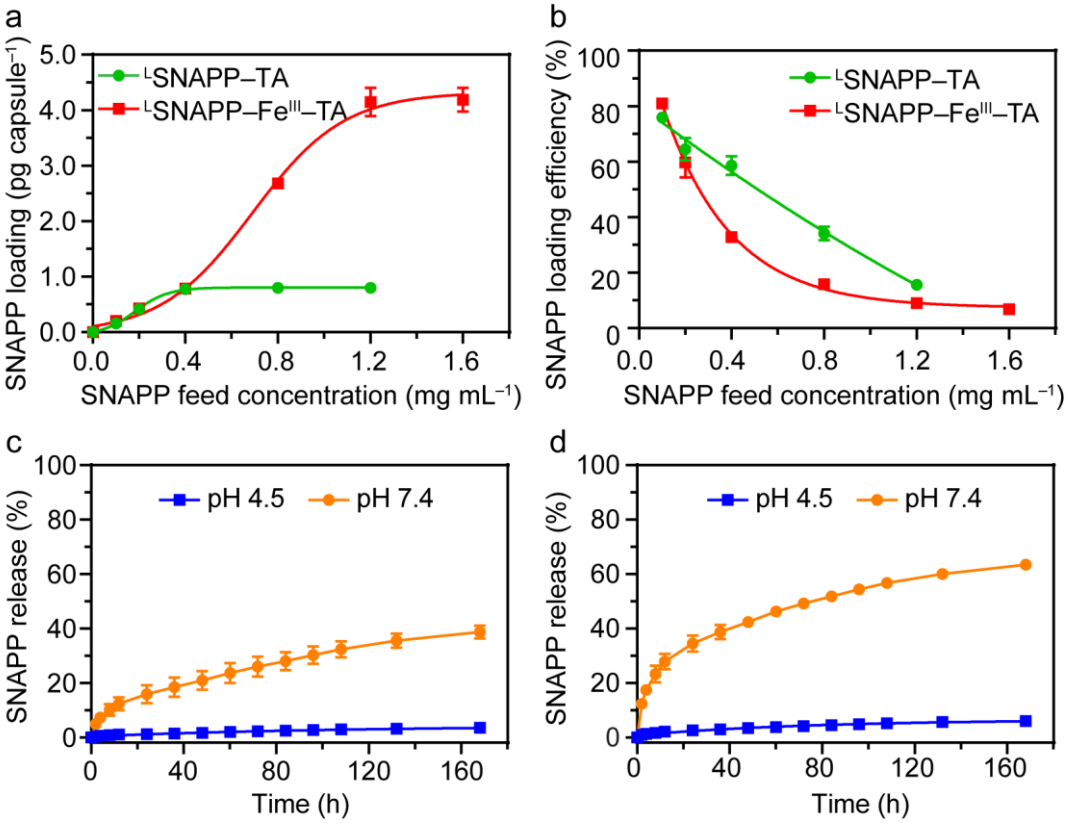

Figure 3. (a) Loading amount and (b) loading efficiency of FITC-labeled ^{L}SNAPPs in ^{L}SNAPP–TA or ^{L}SNAPP–Fe^{III}–TA capsules as a function of ^{L}SNAPP feed concentration. In vitro time-dependent release of FITC-labeled ^{L}SNAPPs from (c) ^{L}SNAPP–Fe^{III}–TA capsules or (d) ^{L}SNAPP–TA capsules at pH 4.5 and 7.4. The results are shown as means ± standard deviations (n = 3).

The in vitro release of SNAPPs from the SNAPP–TA and SNAPP–Fe^{III}–TA capsules was assessed at pH 4.5 and pH 7.4, which represent the intracellular lysosomal pH and extracellular pH, respectively.[44] As shown in Figure 3c,d, a sustained release of ^{L}SNAPPs was achieved at pH 7.4 for both the ^{L}SNAPP–Fe^{III}–TA and ^{L}SNAPP–TA capsules. Although the formation of coordination bonds between polyphenols and metal ions is pH-dependent and MPN capsules composed of Fe^{III} and TA have been found to disassemble at low pH,[32] the presence of SNAPPs may stabilize the MPN capsules via multiple interactions, including

electrostatic interactions, hydrogen bonding (derived from the cationic Lys parts of SNAPPs) and hydrophobic interactions (derived from the hydrophobic Val parts of SNAPPs), with TA or MPNs, as previously reported for protein–polyphenol assemblies.[33] The strong hydrogen bonding and ionic interactions between the Lys residues of SNAPPs and the hydroxyl groups of TA at lower pH may provide the mechanism for the negligible release of SNAPPs observed at acidic pH (4.5) (Figure 3c,d). These interactions may weaken at higher pH, resulting in increased release of SNAPPs at pH 7.4. When incubated at pH 7.4, ~28% of ^{L}SNAPPs was released from the ^{L}SNAPP–TA capsules after 12 h of incubation, which was higher than the ^{L}SNAPPs release (~12%) from the ^{L}SNAPP–Fe^{III}–TA capsules. Furthermore, the SNAPP–TA capsules showed a faster release of SNAPPs and a higher overall release percentage over a period of 168 h than the SNAPP–Fe^{III}–TA capsules for both ^{L}SNAPPs and ^{S}SNAPPs (Figure 3c,d and Figure S9, respectively), probably owing to the thinner capsule shell and the exposure of SNAPPs on the SNAPP–TA capsule surface. However, coating with a thicker MPN layer by using higher concentrations of $FeCl_3 \cdot 6H_2O$ and TA solutions did not significantly further slow the release of SNAPPs from the SNAPP–Fe^{III}–TA capsules (Figure S9 and S10), as the MPN coating is highly porous and allows the diffusion of macromolecules even with high M_w (2000 kDa) through its permeable shell as investigated by incubating the capsules with FITC-dextran of varying molecular weights (3–5, 20, 59–77, 250, 500, and 2000 kDa) (Figure S11). Nevertheless, enhanced release of SNAPPs at physiological pH (pH 7.4) may facilitate a high local concentration of SNAPPs extracellularly upon lung deposition or intracellularly (in the cytoplasm). As SNAPPs specifically affect bacteria and are not cytotoxic toward mammalian cells,[4] drug leakage in non-infected lung tissue is expected to cause negligible adverse effects.

Notably, only ~60% and ~40% of the SNAPPs are released from the SNAPP–TA and SNAPP–Fe^{III}–TA capsules, respectively, at pH 7.4 after 160 h, which suggests that the

remaining SNAPPs are trapped within the capsule shell via additional TA–peptide interactions. Confocal microscopy analysis of the capsules after release of SNAPPs shows that the morphology of the capsules remained spherical and intact after 24 h incubation at 50 mM sodium phosphate buffer pH 7.4 (Figure S12). Although the remaining SNAPPs could reinforce the capsule shell, intracellular conditions, including enzymatic degradation, could further facilitate capsule degradation and SNAPP release.

2.3. In Vitro Antimicrobial Activity

SNAPPs have been found effective against a range of Gram-negative bacteria (*Escherichia coli* (*E. coli*), *Pseudomonas aeruginosa*, *Klebsiella Pneumoniae*, and *Acinetobacter baumannii*).[4] For effective application of the SNAPP-loaded capsules, it is important that the immobilized SNAPPs retain their function (antimicrobial activity) after capsule assembly. Therefore, the antimicrobial activity of the SNAPPs released from the SNAPP–TA and SNAPP–Fe^{III}–TA capsules was evaluated by determining the minimum inhibitory concentration (MIC) values against model Gram-negative bacteria *E. coli* using a standard antimicrobial assay that correlates increases in turbidity of a bacterial culture with bacterial growth.[5] The MIC is the lowest concentration of an antimicrobial agent that prevents visible bacterial growth, with lower MIC values corresponding to stronger antimicrobial activities. Free SNAPP solutions of varying concentrations or released SNAPPs collected from SNAPP–TA or SNAPP–Fe^{III}–TA capsule suspensions at pH 7.4 were added to *E. coli* cultures. Bacteria growth curves at different SNAPP concentrations were obtained by plotting the optical density at 600 nm (OD_{600}) of the samples as a function of time (Figure S13a,c). The OD_{600} of the samples at the time point when bacterial exponential growth was complete for the negative control sample (without SNAPPs) was normalized to the OD_{600} of the negative control (100%), expressed as relative bacterial growth (%). The relative bacterial growth (%) was plotted against the SNAPP concentration and fitted to an exponential regression model

(**Figure 4** and S13b,d). The MIC was determined as the concentration corresponding to 1% relative bacterial growth in the exponential regression. Free ^{L}SNAPPs displayed excellent antimicrobial activity against *E. coli* with an MIC of 16.1 μg mL^{-1}, whereas free ^{S}SNAPPs showed a considerably lower antimicrobial activity (MIC of 134.6 μg mL^{-1}) (Figure S13b,d). The higher antimicrobial activity of ^{L}SNAPPs can be explained by the cooperative mechanism operating among the antimicrobial polypeptides, as reported previously, wherein a higher number of polypeptide arms of SNAPPs can promote cooperative action of neighboring polypeptide arms and thus exert a higher antimicrobial activity.[5] The ^{L}SNAPPs released from the ^{L}SNAPP–TA and ^{L}SNAPP–Fe^{III}–TA capsules retained high antimicrobial activity against *E. coli*, with an MIC of 30.5 μg mL^{-1} for the ^{L}SNAPP–TA capsules and 29.3 μg mL^{-1} for the ^{L}SNAPP–Fe^{III}–TA capsules. The higher MIC values (when compared with that of free ^{L}SNAPPs, 16.1 μg mL^{-1}) are likely due to the presence of some residual TA in the released SNAPPs, which may affect the binding of SNAPPs with bacterial membranes and the subsequent destabilization of bacterial membranes.[45]

Direct comparison with other particles carrying similar antimicrobial agents (antimicrobial peptides) is challenging due to different study conditions and presentation of the data but typical MIC values for other antimicrobial peptide-loaded particle systems, including poly(lactic-*co*-glycolic acid) microparticles and gold nanoparticles range from ~37 mg mL^{-1} (MIC_{90}) to >128 mg mL^{-1} in *E. coli*.[46–48] In comparison, we report MIC values of ~30 mg mL^{-1} for both capsule systems. MIC_{90} represents the MIC value at which ≥90% of the strains within a test population are inhibited. To our knowledge, as the encapsulation of other polymer peptides in delivery systems has not been reported, comparison of our MIC values with other encapsulated polymer peptides is not possible, although free SNAPPs have been found to be orders of magnitude more efficacious when compared with other peptide-based

antimicrobial agents, including magainin II, ovispirin, and melittin, under the same study conditions.[4]

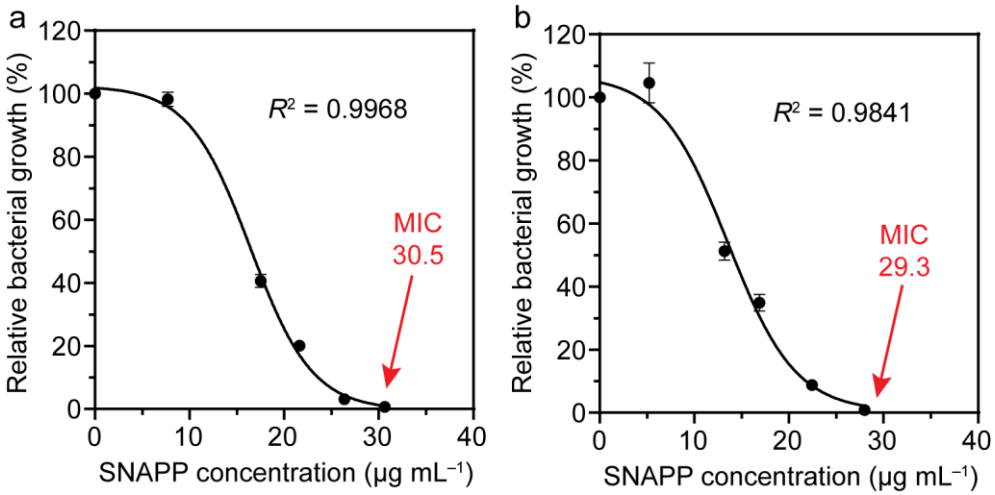

Figure 4. Relative growth (%) of *E. coli* as a function of the concentration of ^{L}SNAPPs released from (a) ^{L}SNAPP–TA or (b) ^{L}SNAPP–Fe^{III}–TA capsules. The MIC, defined as the lowest concentration of SNAPP that inhibited 99% of bacterial growth (i.e., the *X* value at *Y* = 1%), was determined from the fitted exponential regression. The results are shown as means ± standard deviations (*n* = 3).

2.4. Nebulization and Cellular Interactions with Alveolar Macrophages

The potential for antimicrobials to be delivered to the pulmonary region presents opportunities to treat various bacterial infections associated with lung diseases and infections, including cystic fibrosis, tuberculosis, and pneumonia. To demonstrate the potential of ^{L}SNAPP–TA and ^{L}SNAPP–Fe^{III}–TA capsules for pulmonary delivery, we investigated their amenability to the nebulization process by using a commercially available air-jet nebulizer. The nebulizer generates fine inhalable aerosol droplets from a liquid suspension using compressed air (**Figure 5**a) and determines the droplet size distribution even in the presence of particles. Air-jet nebulizers are the standard for the pharmacological testing of formulations containing biomolecules,[49] and hence nebulization is not expected to adversely affect the antimicrobial performance of the capsules. In addition, the size of the capsules (~1.8 μm) is suitable for nebulization and for local delivery to the lungs via inhalation; the capsules are within the size range (1–5 μm aerodynamic diameter) capable of deposition in the deep lung

region.[50] The capsules were nebulized and collected for subsequent characterization. Both ^{L}SNAPP–TA and ^{L}SNAPP–Fe^{III}–TA capsules remained well dispersed in aqueous solution (Figure 5c), suggesting that the particle size distribution is not affected by nebulization, and retained their fluorescence with negligible leakage of SNAPPs (Figure 5b) after nebulization. The morphology and structures of both types of capsules remained intact with no damage or alteration, as observed from the TEM images (Figure 5c), revealing that the physicochemical properties of the ^{L}SNAPP–TA and ^{L}SNAPP–Fe^{III}–TA capsules were unaffected by the nebulization process. These results confirm that the SNAPPs immobilized via the assembly of SNAPP–TA or SNAPP–Fe^{III}–TA capsules can maintain structural integrity during aerosolization process, which is a prerequisite for further investigations on pulmonary delivery applications.

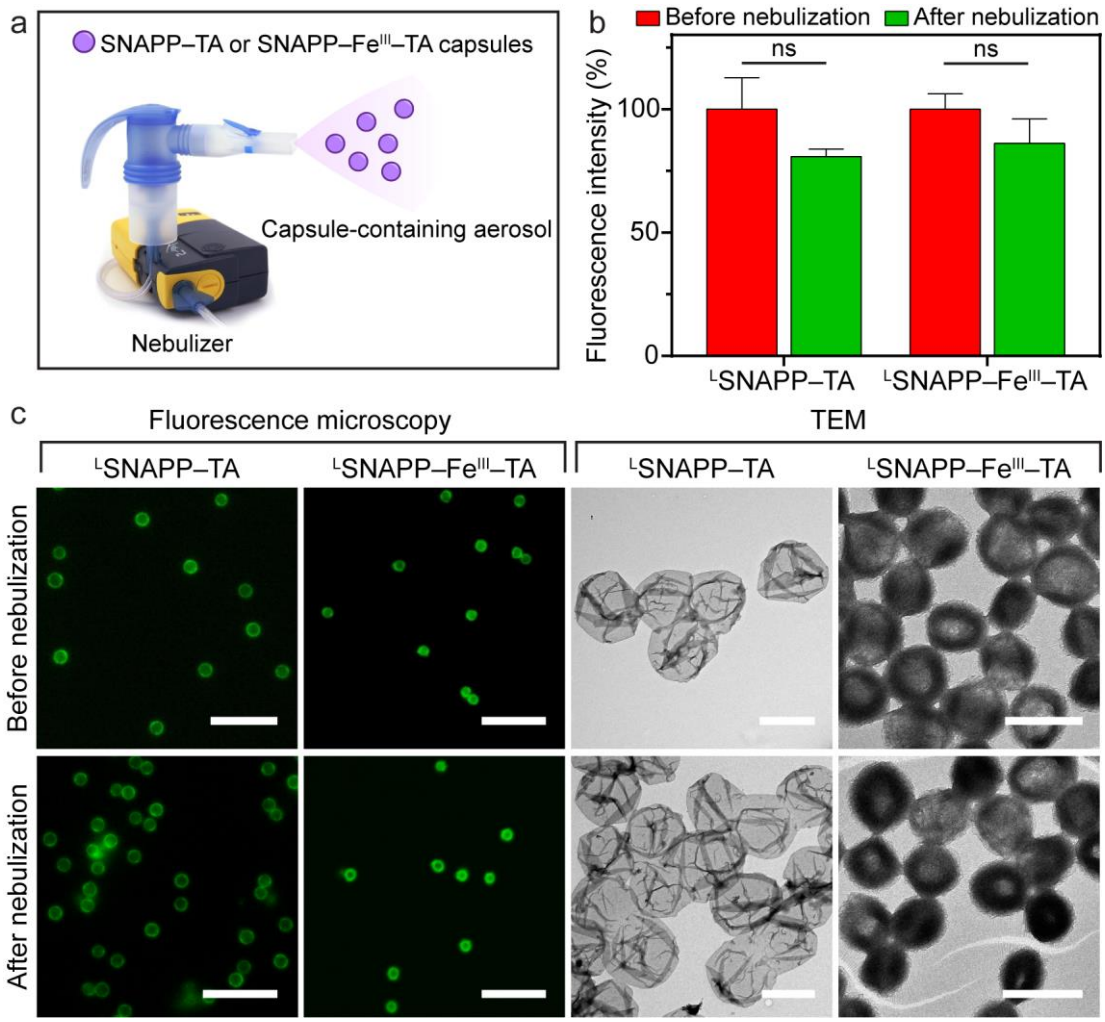

Figure 5. (a) Schematic illustration of the nebulization of SNAPP–TA or SNAPP–Fe^{III}–TA capsule suspensions using a PARI air-jet nebulizer. (b) Fluorescence intensity of ^{L}SNAPP–TA and ^{L}SNAPP–Fe^{III}–TA capsules before and after nebulization. The fluorescence intensity of the capsules before nebulization was normalized to 100% for comparison with those collected after nebulization. The results are shown as means ± standard deviations (n = 3) (two-way ANOVA with Tukey's multiple comparisons test, ns $p > 0.05$). (c) Fluorescence microscopy (scale bars are 10 µm) and TEM (scale bars are 2 µm) images of ^{L}SNAPP–TA and ^{L}SNAPP–Fe^{III}–TA before and after nebulization.

Our previous study on the pulmonary delivery of MPN capsules in mice demonstrated that Fe^{III}–TA-based capsules did not cause overt inflammation or tissue damage in mice and associated primarily with lung resident alveolar macrophages, which, in addition to mucus, are responsible for the clearance of foreign material in the lungs.[40] In the current study, the association of the SNAPP–TA and SNAPP–Fe^{III}–TA capsules with alveolar macrophage was assessed in vitro using a murine alveolar macrophage cell line (MH-S). The SNAPP–TA or SNAPP–Fe^{III}–TA capsules were incubated with MH-S cells over different incubation periods (8 and 24 h) at 37 °C (**Figure 6** and S14). Both types of capsules minimally influenced the viability of MH-S cells after 24 h of incubation as evaluated by a 2,3-bis(2-methoxy-4-nitro-5-sulfophenyl)-2*H*-tetrazolium-5-carboxanilide (XTT) cell viability assay (Figure S15). Despite the similar sizes in aqueous solution (Figure 2a,b,f,g) and similar surface charges at physiological pH (^{L}SNAPP–TA: −28 mV, ^{L}SNAPP–Fe^{III}–TA: −32 mV, as shown in Figure S3), the ^{L}SNAPP–TA capsules exhibited significantly higher association with MH-S cells than the ^{L}SNAPP–Fe^{III}–TA capsules after incubation for 8 h (~37% difference) or 24 h (~52% difference) (Figure 6a), probably due to the thinner capsule shell and resultant higher flexibility and deformability upon contact with the cell membrane, thus leading to greater adhesion to the cell membrane.[51] The differences in the capsule roughness and surface chemistry (presence of SNAPPs on the capsule surface or interior) are also likely to affect cell membrane interaction.[52–54] Note that cell association, as quantified from cell-gated flow cytometry data, refers to the percentage of cells with bound or internalized FITC-labeled particles (i.e., $FITC^{+}$ cells). The internalization of the capsules by the MH-S cells was

assessed by imaging flow cytometry, which enabled imaging of cells in high throughput. As shown in Figure 6b,c, both ^{L}SNAPP–TA and ^{L}SNAPP–Fe^{III}–TA capsules were effectively internalized by the MH-S cells after incubation for 24 h. The cell uptake of ^{L}SNAPP–TA or ^{L}SNAPP–Fe^{III}–TA capsules was confirmed by confocal microscopy (Figure 6d–h). After 8 h of incubation, most of the internalized ^{L}SNAPP–Fe^{III}–TA capsules were intact, retaining their original spherical shape (Figure 6f), whereas some of the ^{L}SNAPP–TA capsules appeared deformed in the cells (Figure 6e). Increasing the incubation time to 24 h resulted in a larger amount of deformed and potentially disassembled ^{L}SNAPP–TA capsules (Figure 6g), whereas most of the ^{L}SNAPP–Fe^{III}–TA capsules remained intact (Figure 6h), indicating that the SNAPP–Fe^{III}–TA capsules were more stable than the SNAPP–TA capsules in the intracellular environment. The deformation and possible disassembly of the SNAPP–TA capsules in macrophages provides potential for tailored intracellular drug release.

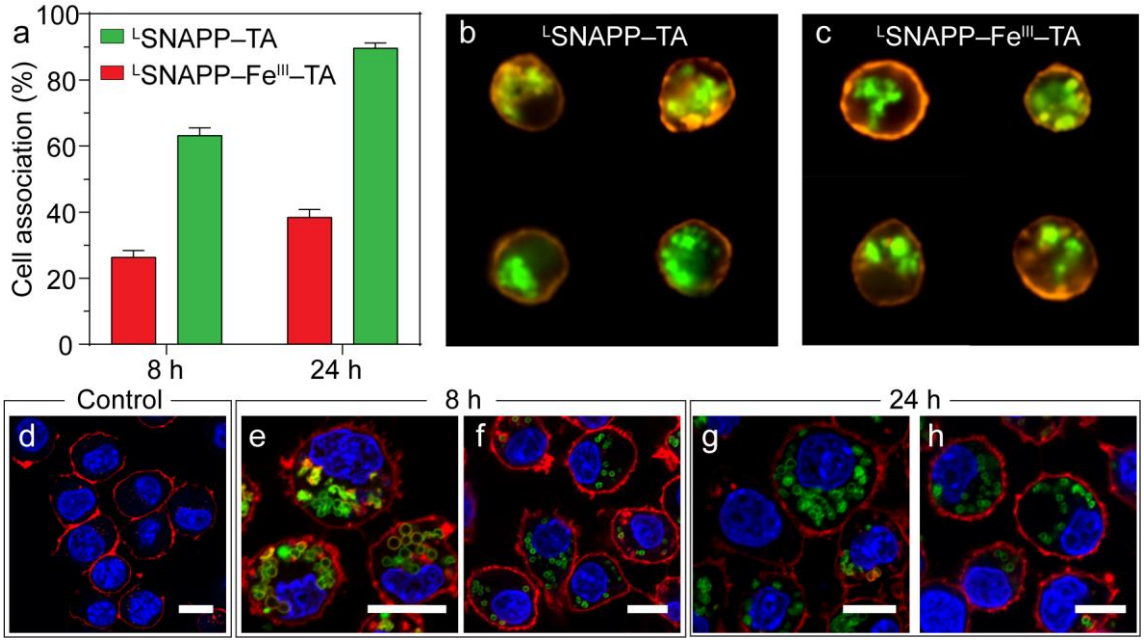

Figure 6. In vitro capsule–cell interaction study. (a) Association of ^{L}SNAPP–TA or ^{L}SNAPP–Fe^{III}–TA capsules with MH-S cells following incubation for 8 or 24 h at 37 °C and a capsule-to-cell ratio of 50:1. The results are shown as means ± standard deviations (n = 3). (b, c) Internalization of ^{L}SNAPP–TA and ^{L}SNAPP–Fe^{III}–TA capsules by MH-S cells after incubation for 24 h at 37 °C and a capsule-to-cell ratio of 50:1 as evaluated by imaging flow cytometry. The capsules were fluorescently labeled by loading with FITC-labeled ^{L}SNAPPs (green) and the cell membranes were stained with wheat germ agglutinin–Alexa Fluor 594 conjugate (WGA-594) (orange). (d–h) Confocal microscopy images of the MH-S cells either in the absence of capsules (d, Control) or incubated with ^{L}SNAPP–TA (e, g) or ^{L}SNAPP–

Fe^{III}–TA (f, h) capsules for 8 h (e, f) or 24 h (g, h) at 37 °C at a capsule-to-cell ratio of 50:1. The capsules were fluorescently labeled by loading with FITC-labeled ^{L}SNAPPs (green). The cell membranes were stained with WGA-594 (red) and the nuclei were stained with Hoechst 33342 (blue). Scale bars are 10 μm in (d–h).

2.5. Intracellular Distribution of SNAPP–TA and SNAPP–Fe^{III}–TA Capsules

To further explore the intracellular and subcellular distributions of the SNAPP–TA and SNAPP–Fe^{III}–TA capsules, we conducted a colocalization analysis of the SNAPP–TA and SNAPP–Fe^{III}–TA capsules with endo/lysosomes in MH-S cells (**Figure 7**). As shown in Figure 7a, after incubation for 24 h with MH-S cells, the ^{L}SNAPP–TA capsules exhibited significant colocalization with endo/lysosomes, indicating that most of the ^{L}SNAPP–TA capsules were entrapped in endo/lysosomal compartments. In contrast, the ^{L}SNAPP–Fe^{III}–TA capsules displayed a lower degree of colocalization with endo/lysosomes, suggesting that the ^{L}SNAPP–Fe^{III}–TA capsules might escape from endo/lysosomal compartments into the cytoplasm, probably due to the “proton-sponge effect” arising from the buffering capacity of MPNs composed of Fe^{III} and TA, as previously reported.[38] The color scatter plots (Figure 7b) and corresponding Pearson’s correlation coefficient (PCC) values (Figure 7c), which provide a statistical correlation between the red and green fluorescence signals in the images, reveal the stronger positive correlation and higher degree of colocalization of the ^{L}SNAPP–TA capsules (PCC ~0.82) with endo/lysosomes when compared with the ^{L}SNAPP–Fe^{III}–TA capsules (PCC ~0.59). These results highlight the potential of the SNAPP–TA capsules for intracellular drug delivery and endo/lysosomal accumulation, which is important as some bacteria (e.g., *Mycobacterium tuberculosis*) commonly reside within endo/lysosomes. Despite the low SNAPP release observed in buffer at pH 4.5 for both capsule systems (Figure 3 c,d), the enzyme-rich environment of the endosomes might facilitate capsule degradation and SNAPP release not easily simulated in vitro.

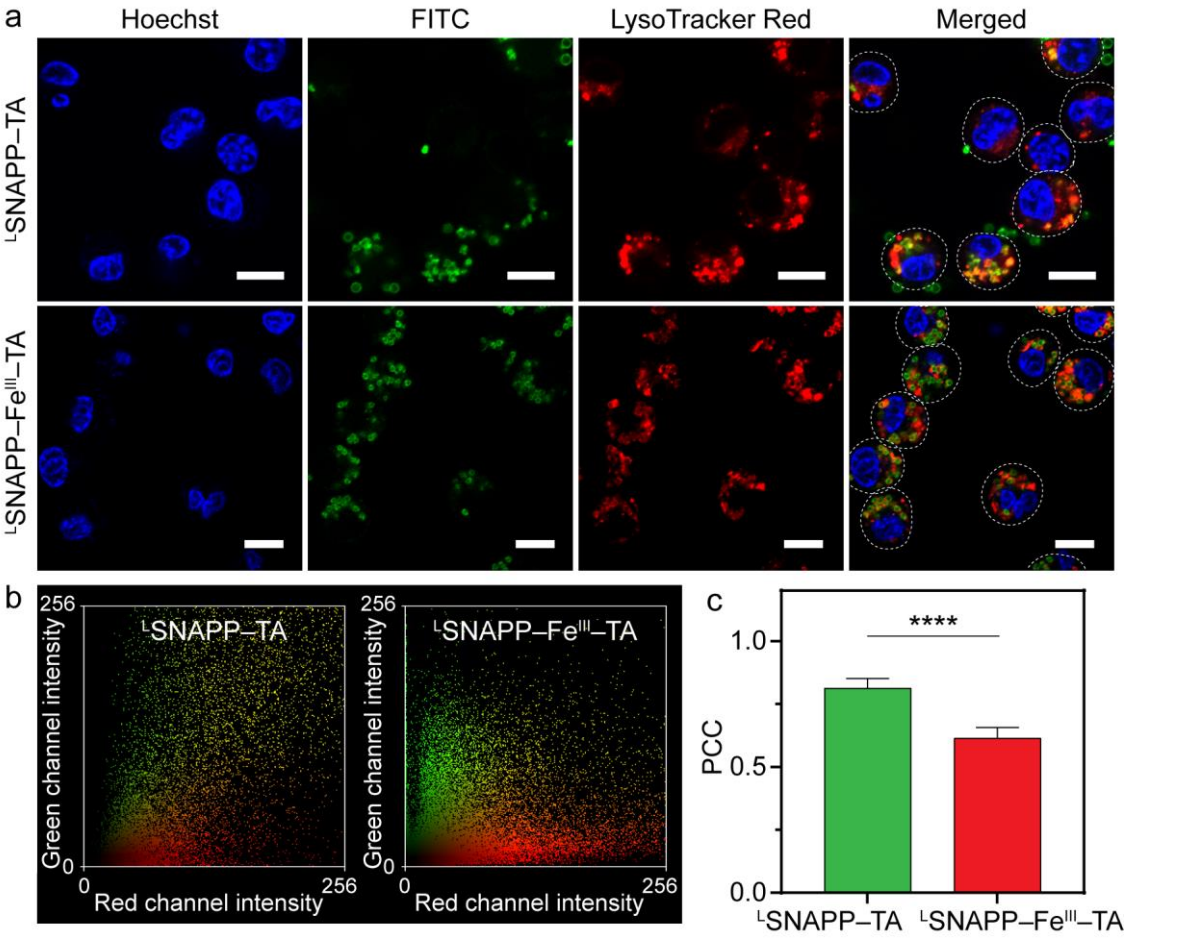

Figure 7. (a) Intracellular distribution of the ^{L}SNAPP–TA and ^{L}SNAPP–Fe^{III}–TA capsules in MH-S cells after incubation for 24 h at 37 °C at a capsule-to-cell ratio of 50:1 as evaluated by confocal microscopy. The capsules were fluorescently labeled by loading with FITC-labeled ^{L}SNAPPs (green). The endo/lysosomes were stained with LysoTracker Red (red). The nuclei were stained with Hoechst 33342 (blue). The dashed lines in the merged images indicate the cellular boundaries based on the corresponding bright-field images. Scale bars are 10 μm. (b) Representative color scatter plots of the ^{L}SNAPP–TA and ^{L}SNAPP–Fe^{III}–TA capsules vs endo/lysosomes. (c) Corresponding PCC values of the ^{L}SNAPP–TA and ^{L}SNAPP–Fe^{III}–TA capsules vs endo/lysosomes (means ± standard deviations, $n > 50$). **** $p < 0.0001$ from the student *t*-test.

3. Conclusion

We demonstrated the immobilization of antimicrobial SNAPPs in polyphenol-based microcapsules using a templated assembly approach. SNAPP–TA and SNAPP–Fe^{III}–TA capsules were assembled via TA and SNAPP complexation in the absence or presence of Fe^{III} to achieve a maximum ^{L}SNAPP loading of 0.8 and 4.4 pg per capsule, respectively. Both SNAPP–TA and SNAPP–Fe^{III}–TA capsules displayed a sustained release of SNAPPs at pH 7.4, with the SNAPP–TA capsules showing faster release within 12 h and greater overall

release over a prolonged period (168 h) than the SNAPP–Fe^{III}–TA capsules. The ^{L}SNAPPs released from ^{L}SNAPP–TA and ^{L}SNAPP–Fe^{III}–TA capsules retained high antimicrobial activity with MIC of 30.5 and 29.3 μg mL^{-1}, respectively, as evaluated using an *E. coli* model. The capsules maintained their morphology after nebulization, which was performed to assess their potential for pulmonary delivery. Cell-associated SNAPP–TA and SNAPP–Fe^{III}–TA capsules were efficiently internalized in vitro by MH-S murine alveolar macrophages with negligible cytotoxicity. The ^{L}SNAPP–TA capsules showed appreciable colocalization with endo/lysosomes (~30% higher PCC value than that obtained for ^{L}SNAPP–Fe^{III}–TA capsules), suggesting their potential to kill bacteria that commonly reside within endo/lysosomes of alveolar macrophages (e.g., *Mycobacterium tuberculosis*). This study demonstrates the prospect for pulmonary delivery of antimicrobial SNAPP capsules to treat respiratory diseases caused by bacterial infection, including pneumonia and tuberculosis. Moreover, the template-mediated assembly of SNAPP–TA and SNAPP–Fe^{III}–TA capsules described in the present study, using small and large SNAPPs, may prove useful for the immobilization or encapsulation of other peptide-based drugs or drug payloads for the therapy of lung diseases via pulmonary (or other) delivery routes.

4. Methods

Materials: Poly(sodium 4-styrenesulfonate) (PSS, 70 kDa), calcium nitrate tetrahydrate ($Ca(NO_3)_2 \cdot 4H_2O$), sodium carbonate (Na_2CO_3), $FeCl_3 \cdot 6H_2O$, TA, MOPS, EDTA, Dulbecco's phosphate-buffered saline (DPBS), glycine hydrochloride, sodium acetate, sodium phosphate monobasic monohydrate, sodium phosphate dibasic, sodium borohydride, G2 PAMAM dendrimer, bis(trichloromethyl)carbonate (triphosgene), trifluoroacetic acid (TFA), HBr (33% in acetic acid), anhydrous *n*-pentane, FITC, paraformaldehyde, phenazine methosulfate (PMS), methanol, anhydrous dimethyl sulfoxide (DMSO), *N*,*N*-dimethylformamide (DMF), 2-mercaptoethanol, FITC-dextran (3–5, 20, 59–77, 250, 500, and 2000 kDa), and Mueller–

Hinton broth (MHB) were purchased from Sigma-Aldrich (Australia). Dulbecco's modified Eagle's medium (DMEM), RPMI-1640 media, fetal bovine serum (FBS), WGA-594, Hoechst 33342, and LysoTracker Red DND-99 were purchased from Life Technologies (Australia). XTT was purchased from Invitrogen (Australia). H-L-Lys(*Z*)-OH (>99%) was purchased from Mimotopes (Australia). D,L-Val (>99%) was purchased from Acros Organics (Australia). G0 PAMAM dendrimer was purchased from Dendritech Inc. (USA). Sodium bicarbonate ($NaHCO_3$), tetrahydrofuran (THF), diethyl ether, ethyl acetate (EtOAc), and *n*-butyl alcohol were purchased from Chem-Supply (Australia). High-purity water with a resistivity greater than 18.2 MΩ cm, which was used in all experiments, was obtained from a three-stage Millipore Milli-Q plus 185 purification system (Millipore Corporation).

Synthesis of SNAPPs: Synthesis of D,L-Valine N-Carboxyanhydrides (Val NCA) and (Z)-L-Lysine N-Carboxyanhydrides (Lys NCA). Val NCA and Lys NCA were synthesized using a previously reported method.[5] Briefly, dried H-L-Lys(*Z*)-OH (2 g, 7.14 mmol) or D,L-Val (2 g, 17.0 mmol) was dissolved in anhydrous THF (50 mL) under argon, followed by the addition of triphosgene (for Lys NCA: 0.85 g, 2.86 mmol, 1.2 equiv. phosgene; for Val NCA: 2.0 g, 6.74 mmol, 1.2 equiv. phosgene) to the suspension. The mixture was refluxed at 65 °C for 2 h with constant stirring. The clear solution was sparged with argon for 45 min. After cooling to room temperature, a solid was obtained. The solid was then resuspended in anhydrous EtOAc (50 mL) and placed in a separating funnel where the crude NCA solution was removed by gently washing with chilled saturated brine solution (50 mL) and 0.5% w/v $NaHCO_3$ solution (50 mL). The organic phase was dried with $MgSO_4$ followed by filtering and concentrating into an oil under low heat, and then recrystallized twice from anhydrous EtOAc and anhydrous *n*-pentane. The resulting crystals were further filtered and washed with dry *n*-pentane, and subsequently redissolved in minimal EtOAc, filtered, precipitated, washed with dry *n*-pentane, and dried at ambient temperature to afford a white powder of Val NCA or Lys

NCA (yield ~80%). Lys NCA – ^{1}H NMR (400 MHz, $CDCl_3$, δ_H): 1.40–1.60 (m, 4H, NH–CH_2–CH_2–CH_2–CH_2–), 1.81–1.94 (m, 2H, NH–CH_2–CH_2–CH_2–CH_2–), 3.18 (m, 2H, NH–CH_2–CH_2–CH_2–CH_2–), 4.25 (t, 1H, *J* = 4.0 Hz, CHN), 4.97 (s, 1H, side chain NH), 5.09 (s, 2H, CH_2–ArH), 7.04 (s, 1H, ring NH), 7.3–7.4 (m, 5H, ArH). mp 80–82 °C (lit.[55] mp 80 °C). Val NCA – ^{1}H NMR (400 MHz, $CDCl_3$, δ_H): 1.02 (d, 3H, *J* = 8.0 Hz, CH_3), 1.08 (d, 3H, *J* = 8.0 Hz, CH_3), 2.25 (m, 1H, $CH(CH_3)_2$), 4.22 (d, 1H, *J* = 4.0 Hz, CH–NH), 6.95 (s, 1H, CO–NH). mp 99–100 °C (lit.[45] mp 99 °C).

Synthesis of Poly(Z-L-Lys-r-D,L-Val)$_{arm}$PAMAM-$(NH_2)_{m,core}$ Star Peptide Polymers. Lys NCA and Val NCA at a molar ratio of 2:1 were dissolved in anhydrous DMF with a total NCA concentration of ~55 mg mL^{-1}. The solution was added to a test tube containing PAMAM-$(NH_2)_m$ (dried) dissolved completely in anhydrous DMSO (volume corresponding to 10% v/v of final reaction volume) under N_2. The tube was then immersed in an ice chest and stirred for 24 h under constant nitrogen flow and with a bleed for CO_2 removal. *n*-Butyl alcohol (0.86 µL mg^{-1} of NCA_{total}) was then added to the mixture and stirred for 1 h to quench the remaining NCA monomer. The resulting mixture was concentrated under vacuum followed by precipitation in diethyl ether. The precipitate was then washed thoroughly with ether and dried in a vacuum to afford poly(*Z*-L-Lys-*r*-D,L-Val)$_{arm}$PAMAM-$(NH_2)_{m,core}$ star peptide polymers as an off-white solid. The average yield was ~60%.

Deprotection of Star Peptide Polymers. The star peptide polymers synthesized as described above was completely dissolved in TFA (200 mg mL^{-1}) followed by the addition of 33% HBr in acetic acid (10 mL g^{-1} peptide polymers). After stirring for 2 h at room temperature, the mixture was allowed to precipitate in diethyl ether and subsequently washed with ether twice followed by drying under vacuum. The resulting solid was redissolved in minimal Milli-Q water and thoroughly dialyzed against Milli-Q water in a 3.5 kDa dialysis tubing. The

dialyzed solution was lyophilized to obtain the deprotected SNAPP as a dried white solid. ^{1}H NMR (400 MHz, D_2O, δ_H): 0.9 (s, 2$(CH)_3$), 1.3–1.9 (m, NH–CH_2–CH_2CH_2–CH_2–), 2.0 (br s, CH–NH valine), 3.0 (s, NH–CH_2–CH_2–CH_2–CH_2–), 4.0–4.15 (s, CH–NH backbone valine), 4.2–4.4 (s, CH–NH backbone lysine).

FITC Labeling of SNAPPs: SNAPPs (40 mg, 146 µmol amine) and triethylamine (4.1 µL, 30 µmol, 20 mol% amine) were added to anhydrous DMSO (600 µL) under N_2, followed by stirring for 30 min for complete dissolution of SNAPPs. FITC (5.6 mg, 14.4 µmol, 10 mol% amine) dissolved in anhydrous DMSO (600 µL) was then added to the above mixture followed by stirring under N_2 at room temperature in the dark for 20 h. Two drops of 1 M HCl were then added to reprotonate any remaining free Lys amines. ^{S}SNAPP or ^{L}SNAPP reaction mixture was dialyzed using 1 kDa or 3.5 kDa dialysis tubing, respectively, against methanol over 48 h in the dark. The dialyzed content was then concentrated, redissolved in minimal methanol, and precipitated in ether, followed by washing with ether and drying under low vacuum in the dark overnight, resulting in FITC-labeled SNAPPs.

Synthesis of $CaCO_3$ Particles: $CaCO_3$ particles with an average diameter of 1.8 ± 0.1 µm were synthesized by a fast precipitation method in the presence of PSS, followed by removal of organic material by calcination.[40] To prepare PSS-stabilized $CaCO_3$ particles, $Ca(NO_3)_2$ solution (5 mL, 1 M), PSS solution (20 mL, 10 mg mL^{-1}), and Milli-Q water (175 mL) were mixed in a 200 mL beaker under mild stirring. Next, Na_2CO_3 solution (1 mL, 1 M), PSS solution (0.5 mL, 10 mg mL^{-1}), and Milli-Q water (3.5 mL) were mixed in a 50 mL tube. These two solutions were mixed in a 200 mL beaker under vigorous stirring for 1 min. After static incubation for 20 min, the mixed solution was further vigorously stirred for 1 min. The obtained particles were washed three times with Milli-Q water by centrifugation (2000*g*, 2 min), dried in an oven, and calcined in air at 450 °C for 6.5 h.

Synthesis of SNAPP–TA Capsules: For the assembly of SNAPP–TA capsules, TA solution (5 µL, 40 mg mL^{-1}) was added to $CaCO_3$ particles (2 mg) that were dispersed in Milli-Q water (140 µL). After 15 min of incubation under shaking (1400 rpm), SNAPP solution (50 µL, 2 mg mL^{-1}) was added to the mixture followed by incubation for 6 h at 37 °C with shaking (1400 rpm). The particles were washed three times with Milli-Q water to remove excess TA and SNAPPs (1000*g*, 1.5 min). The SNAPP–TA capsules were obtained after removal of $CaCO_3$ templates using EDTA (100 mM, pH 8.0). For capsule imaging and the quantification of the loading and release of SNAPPs, FITC-labeled SNAPPs were used.

Synthesis of SNAPP–Fe^{III}–TA Capsules: To assemble SNAPP–Fe^{III}–TA capsules, a $CaCO_3$ particle suspension (20 µL, 100 mg mL^{-1}) was diluted to 100 µL with Milli-Q water and incubated with SNAPP solution (150 µL, 2 mg mL^{-1}) for 2 h under shaking (1400 rpm) to allow the infiltration and adsorption of SNAPPs onto the $CaCO_3$ particles. The particles were then washed three times with Milli-Q water to remove free SNAPPs. Then, $FeCl_3 \cdot 6H_2O$ solution (5 µL, 10 mg mL^{-1}) and TA solution (5 µL, 40 mg mL^{-1}) were sequentially added to the SNAPP-loaded $CaCO_3$ particle suspension to form metal–polyphenol complexes. The mixture was vigorously vortexed for 10 s, after which MOPS buffer (500 µL, 50 mM, pH 8.0) was added to raise the pH. The particles were washed three times with Milli-Q water to remove excess TA and metal ions (1000*g*, 1.5 min). The SNAPP–Fe^{III}–TA capsules were obtained after removal of $CaCO_3$ templates using EDTA (100 mM, pH 8.0). For the preparation of thick SNAPP–Fe^{III}–TA capsules (i.e., SNAPP–Fe^{III}–TA (thick) capsules), a slightly modified protocol was applied: $FeCl_3 \cdot 6H_2O$ solution (20 µL, 10 mg mL^{-1}), TA solution (40 µL, 40 mg mL^{-1}), and MOPS buffer (500 µL, 50 mM, pH 8.0) were sequentially added to the SNAPP-loaded $CaCO_3$ particle suspension, followed by washing six times with Milli-Q water (1000*g*, 1.5 min). The templates were removed following the same method as

described above. To enable capsule imaging and quantification of the loading and release of SNAPPs by fluorescence, FITC-labeled SNAPPs were used.

Capsule Characterization: Fluorescence microscopy images were taken with an Olympus IX71 inverted fluorescence microscope equipped with a DIC slider (U-DICT, Olympus), the corresponding filter sets, and a 60× or 100× oil immersion objective (Olympus UPFL20/0.5NA, W.D. 1.6). TEM images were taken with an FEI Tecnai TF20 instrument operating at an operation voltage of 120 kV. The TEM samples were prepared by dropping an aqueous capsule suspension onto a plasma-treated formvar-coated copper grid and subsequent drying in air. AFM images were acquired using a NanoWizard II AFM instrument (JPK Instruments, Berlin, Germany). An aqueous suspension of the capsules was placed onto Piranha-precleaned glass slides and then dried in air. *Caution! Piranha solution is extremely corrosive and reacts violently with organic materials. It should be handled with great care.* When air-dried, the capsules collapse, and the minimum height of the collapsed flat region of the capsules is measured relative to the glass substrate using tapping mode AFM. This height represents the double-wall thickness of the capsule (sphere), and hence the single-wall (shell) thickness is obtained by dividing the capsule height by two.[31] SEM images were captured with a Philips XL30 instrument at an operation voltage of 15 kV. The SEM samples were prepared by dropping a capsule suspension onto a silicon wafer, followed by sputter-coating with gold. The ζ-potential of the capsules was measured by a Zetasizer Nano-ZS instrument (Malvern Instruments, Malvern, UK). Capsule counting was performed by flow cytometry (Apogee Flow, UK). Image analysis was conducted using ImageJ software.

SNAPP Loading Capacity of SNAPP–TA and SNAPP–Fe^{III}–TA Capsules: To assess the SNAPP loading capacity of the SNAPP–TA and SNAPP–Fe^{III}–TA capsules, FITC-labeled SNAPP solutions of varying concentrations were used for the assembly of SNAPP–TA and

SNAPP–Fe^{III}–TA capsules. The UV absorbance at 498 nm of the diluted SNAPP–TA or SNAPP–Fe^{III}–TA capsule suspensions was measured on an Infinite M200 microplate reader (Tecan, Switzerland), and the concentration of immobilized SNAPPs was calculated using a standard curve, which was calibrated by measuring SNAPP solutions with different known concentrations. Capsule counting was performed by flow cytometry. The loading capacity was expressed in picograms of SNAPPs per capsule, and the loading efficiency was expressed as a percentage of the amount of immobilized SNAPPs relative to the amount of SNAPPs in the feed solution.

In Vitro SNAPP Release: In vitro time-dependent release of SNAPPs from SNAPP–TA and SNAPP–Fe^{III}–TA capsules was measured as follows: SNAPP–TA or SNAPP–Fe^{III}–TA capsules prepared from FITC-labeled SNAPPs were suspended in sodium acetate buffer (150 µL, 50 mM, pH 4.5) or sodium phosphate buffer (50 mM, pH 7.4) under shaking (1000 rpm) at 37 °C. At predefined time points, capsules in the buffers were centrifuged (SNAPP–TA: 3000*g*, 5 min; SNAPP–Fe^{III}–TA: 1000*g*, 2.5 min) and the supernatant (100 µL) was collected for fluorescence intensity measurements by an Infinite M200 microplate reader (Tecan, Switzerland) at an excitation wavelength of 490 nm and an emission wavelength of 525 nm. The SNAPP concentration in the supernatant was calculated according to the standard curve established from measuring the absorbance of SNAPP solutions at varying known concentrations. The capsule suspensions were topped up with the corresponding fresh buffer solutions (100 µL) to maintain a total volume of 150 µL for the subsequent release study.

Capsule Permeability Measurements: Capsule permeability was evaluated according to a previously reported method.[31] The suspensions of SNAPP–TA or SNAPP–Fe^{III}–TA capsules (~1×10^7 capsules mL^{-1}) in different buffers (the same buffers as those used in the SNAPP release study) were mixed with an equal volume of FITC-dextran solution (5 mg mL^{-1}) in the

corresponding buffers. Confocal microscopy images of the capsules were taken after incubating the capsules with FITC-dextran solutions for 15 min in the dark. Capsules with dark interiors were considered to be impermeable, whereas capsules with interiors of similar fluorescent intensity to the outer environment were considered to be permeable. At least 100 capsules were assessed for each sample.

In Vitro Antimicrobial Activity: To assess the antimicrobial activity of the SNAPPs released from the capsules compared with free SNAPPs, *E. coli* was used for the antimicrobial assay based on a standard method with slight modifications.[5] *E. coli* (American Type Culture Collection (ATCC) 14948) was incubated in MHB at 37 °C under orbital shaking (200 rpm) for 5 h to allow bacteria growth to proceed. The bacteria were then dispersed in DMEM to achieve a concentration of 3×10^6 cells mL^{-1}, after which the *E. coli* suspension (150 µL) was added to a 96-well microplate. Then, 150 µL of serial two-fold dilutions of free SNAPP solutions (400−3.12 mg mL^{-1}) or released SNAPPs collected from capsule suspensions at pH 7.4 was added to the microplate, resulting in a mixture (300 µL) of bacteria and SNAPPs. A sample of bacteria that was not treated with SNAPPs was set as a negative control. After incubation for 90 min at 37 °C, the mixture (100 µL) of the bacteria and SNAPP was incubated with the same volume of MHB on a microplate. The microplate was incubated at 37 °C under orbital shaking (180 rpm) on an Infinite M200 microplate reader (Tecan, Switzerland), and the OD_{600} of the samples was measured every 20 min for at least 7 h. The OD_{600} of the samples at the time point when bacterial exponential growth was complete for the negative control sample (without SNAPPs) was normalized to the OD_{600} of the negative control (100%), expressed as relative bacterial growth (%). The relative bacterial growth (%) was plotted against the SNAPP concentration and fitted to an exponential regression. The MIC was determined as the concentration corresponding to 1% relative bacterial growth in the exponential regression.

Nebulization of SNAPP–TA and SNAPP–Fe^{III}–TA Capsules: To investigate the amenability of the capsules to nebulization process, an aliquot (2 mL) of SNAPP–TA or SNAPP–Fe^{III}–TA capsule suspension was subjected to nebulization for 5 min using a PARI air-jet nebulizer. The outlet of the nebulizer was attached to a pipette tip to direct the flow of aerosol into a 1.5 mL Eppendorf tube for aerosol collection. The collected capsules were directly used for characterization.

Cell Culture: Mouse alveolar macrophage MH-S cells (ATCC, USA) were cultured in complete RPMI-1640 media containing 10% FBS and 0.05 mM 2-mercaptoethanol at 37 °C with 5% CO_2 in a humidified atmosphere.

Cell Viability Analysis by XTT Assay: The cytotoxicity of the capsules was evaluated by using an XTT cell viability assay. MH-S cells cultured in a 96-well plate (1×10^4 cells per well) were treated with SNAPP–TA or SNAPP–Fe^{III}–TA capsules (without FITC label) at a capsule-to-cell ratio of 10:1 or 50:1 for 24 h at 37 °C. After incubation, the cell culture media was replaced with fresh RPMI-1640 media (100 µL) containing XTT and PMS (9 mL of 0.2 mg mL^{-1} XTT in RPMI-1640 media and 22.5 µL of 0.6 mg mL^{-1} PMS in DPBS). After further incubation for 4 h, the absorbance of the mixture at 475 nm was measured using an Infinite M200 microplate reader (Tecan, Switzerland). The relative cell viability (%) was expressed as a percentage of the absorbance of the treated cells relative to the untreated cells.

Cell Association Analysis by Flow Cytometry: MH-S cells were seeded in a 24-well plate (8×10^4 cells per well) in RPMI-1640 media with 10% (v/v) FBS and 0.05 mM 2-mercaptoethanol and cultured overnight. SNAPP–TA or SNAPP–Fe^{III}–TA capsules were added to the cell culture at a capsule-to-cell ratio of 50:1. After incubation for 8 or 24 h at 37 °C, the cells were

washed twice with DPBS and harvested by trypsinization via centrifugation (100*g*, 10 min). The cell pellets were washed with DPBS three times and finally resuspended in DPBS (250 μL) for the cell association analysis by flow cytometry (Apogee Flow). Three independent experiments were performed with at least 8000 cells analyzed in each individual experiment.

Cell Association Imaging by Confocal Microscopy: MH-S cells were seeded in a 8-well Lab-Tek chambered coverglass slides (Thermo Fisher Scientific, USA) (4×10^4 cells per well) in RPMI-1640 media with 10% (v/v) FBS and 0.05 mM 2-mercaptoethanol and treated with SNAPP–TA or SNAPP–Fe^{III}–TA capsules at a capsule-to-cell ratio of 50:1. After incubation for 8 or 24 h at 37 °C, the cells were gently washed with DPBS and then fixed with paraformaldehyde (4 % in DPBS) for 15 min at room temperature. The fixed cells were then stained with WGA-594 (5 μg mL^{-1}) for 5 min in the dark and Hoechst 33342 (1 μg mL^{-1}) for 5 min at room temperature. Cell association imaging was performed using a Nikon A1R+ laser scanning confocal microscope (Nikon Corporation, Japan) equipped with a Plan Apo λ 60× 1.4 NA oil immersion objective and 405, 488, 561, and 640 nm lasers, and analyzed by ImageJ software.

Cell Internalization Analysis by Imaging Flow Cytometry: MH-S cells were seeded in a 6-well plate (2×10^5 cells per well) in RPMI-1640 media with 10% (v/v) FBS and 0.05 mM 2-mercaptoethanol and incubated overnight. SNAPP–TA or SNAPP–Fe^{III}–TA capsules were added to the cell culture at a capsule-to-cell ratio of 50:1. After incubation for 24 h at 37 °C, the cells were washed twice with DPBS and harvested by trypsinization by centrifugation (100*g*, 10 min). The cells were then washed with DPBS three times and fixed with paraformaldehyde (4 % in DPBS) for 15 min at room temperature. The fixed cells were then stained with WGA-594 (5 μg mL^{-1}) for 5 min in the dark at room temperature and finally resuspended in DPBS (50 μL) for cell internalization analysis by imaging flow cytometry

(AMNIS ImageStream®X MarkII, Amnis Corporation, USA). Bright-field and fluorescence images of at least 5000 cells were obtained.

Colocalization Analysis by Confocal Laser Scanning Microscopy: MH-S cells were seeded in an 8-well Lab-Tek chambered coverglass slides (Thermo Fisher Scientific, USA) (4×10^4 cells per well) in RPMI-1640 media with 10% (v/v) FBS and 0.05 mM 2-mercaptoethanol and allowed to incubate overnight. SNAPP–TA or SNAPP–Fe^{III}–TA capsules were added to the culture media at a capsule-to-cell ratio of 50:1. After incubation for 24 h at 37 °C, the cells were gently washed three times with DPBS and then incubated with 100 nM LysoTracker Red DND-99 for 1 h according to the standard protocol for endo/lysosome staining from the supplier. Cells were then gently washed twice with DPBS and incubated with Hoechst 33342 (1 μg mL^{-1}) for 10 min for nuclei staining. The live cells were imaged using a Nikon A1R confocal microscope equipped with a 60× oil immersion objective. PCC values and color scatter plots were analyzed using WCIF ImageJ software. The experiments were repeated in triplicates and representative images with more than 50 cells were used to calculate the PCC values. The results are presented as means ± standard deviations.

Minimum Information Reporting in Bio–Nano Experimental Literature (MIRIBEL): The studies conducted herein, including material characterization, biological characterization, and experimental details, conform to the MIRIBEL reporting standard for bio–nano research,[56] and we include a companion checklist of these components in the Supporting Information.

Supporting Information
Supporting Information is available from the Wiley Online Library or from the author.

Acknowledgements
This research was conducted and funded by the Australian Research Council Centre of Excellence in Convergent Bio-Nano Science and Technology (project number CE140100036). F.C. acknowledges the award of a National Health and Medical Research Council Senior

Principal Research Fellowship (GNT1135806). C.C.-J. acknowledges the award of a Melbourne Research Fellowship (The University of Melbourne). S.J.S. acknowledges the award of an Early Career Research Grant (Melbourne School of Engineering, The University of Melbourne). This work was performed in part at the Materials Characterization and Fabrication Platform (MCFP) at The University of Melbourne, the Victorian Node of the Australian National Fabrication Facility (ANFF), and the Biosciences Microscopy Facility at The University of Melbourne. We acknowledge Y. Han and J. Chen for assistance with experiments and helpful discussions.

Received: ((will be filled in by the editorial staff))
Revised: ((will be filled in by the editorial staff))
Published online: ((will be filled in by the editorial staff))

References

[1] R. P. Dickson, J. R. Erb-Downward, H. C. Prescott, F. J. Martinez, J. L. Curtis, V. N. Lama, G. B. Huffnagle, *Microbiome* **2014**, *2*, 28.

[2] J. F. Chmiel, T. R. Aksamit, S. H. Chotirmall, E. C. Dasenbrook, J. S. Elborn, J. J. LiPuma, S. C. Ranganathan, V. J. Waters, F. A. Ratjen, *Ann. Am. Thorac. Soc.* **2014**, *11*, 1120.

[3] S. R. Shrivastava, P. S. Shrivastava, J. Ramasamy, *J. Res. Med. Sci.* **2015**, *20*, 718.

[4] S. J. Lam, N. M. O'Brien-Simpson, N. Pantarat, A. Sulistio, E. H. Wong, Y. Y. Chen, J. C. Lenzo, J. A. Holden, A. Blencowe, E. C. Reynolds, G. G. Qiao, *Nat. Microbiol.* **2016**, *1*, 16162.

[5] S. J. Shirbin, I. Insua, J. A. Holden, J. C. Lenzo, E. C. Reynolds, N. M. O'Brien-Simpson, G. G. Qiao, *Adv. Healthcare Mater.* **2018**, *7*, 1800627.

[6] M. Hoppentocht, P. Hagedoorn, H. W. Frijlink, A. H. de Boer, *Eur. J. Pharm. Biopharm.* **2014**, *86*, 23.

[7] N. P. Mortensen, P. Durham, A. J. Hickey, *J. Microencapsulation* **2014**, *31*, 785.

[8] J. S. Patton, P. R. Byron, *Nat. Rev. Drug Discovery* **2007**, *6*, 67.

[9] S. Azarmi, W. H. Roa, R. Lobenberg, *Adv Drug Delivery Rev.* **2008**, *60*, 863.

[10] J. C. Sung, B. L. Pulliam, D. A. Edwards, *Trends Biotechnol.* **2007**, *25*, 563.

[11] A. S. Silva, A. M. Sousa, R. P. Cabral, M. C. Silva, C. Costa, S. P. Miguel, V. D. B. Bonifacio, T. Casimiro, I. J. Correia, A. Aguiar-Ricardo, *Int. J. Pharm.* **2017**, *529*, 240.

[12] Y. Malam, M. Loizidou, A. M. Seifalian, *Trends Pharmacol. Sci.* **2009**, *30*, 592.

[13] P. Tanner, P. Baumann, R. Enea, O. Onaca, C. Palivan, W. Meier, *Acc. Chem. Res.* **2011**, *44*, 1039.

[14] U. Kedar, P. Phutane, S. Shidhaye, V. Kadam, *Nanomedicine* **2010**, *6*, 714.

[15] P. Kesharwani, K. Jain, N. K. Jain, *Prog. Polym. Sci.* **2014**, *39*, 268.

[16] P. P. Yang, S. L. Gai, J. Lin, *Chem. Soc. Rev.* **2012**, *41*, 3679.

[17] J. Cui, J. J. Richardson, M. Bjornmalm, M. Faria, F. Caruso, *Acc. Chem. Res.* **2016**, *49*, 1139.

[18] Y. J. Wang, Y. Yan, J. W. Cui, L. Hosta-Rigau, J. K. Heath, E. C. Nice, F. Caruso, *Adv. Mater.* **2010**, *22*, 4293.

[19] J. K. Patra, G. Das, L. F. Fraceto, E. V. R. Campos, M. D. P. Rodriguez-Torres, L. S. Acosta-Torres, L. A. Diaz-Torres, R. Grillo, M. K. Swamy, S. Sharma, S. Habtemariam, H. S. Shin, *J. Nanobiotechnol.* **2018**, *16*, 71.

[20] V. P. Torchilin, *Nat. Rev. Drug Discovery* **2014**, *13*, 813.

[21] J. Majumder, O. Taratula, T. Minko, *Adv. Drug Delivery Rev.* **2019**, *144*, 57.

[22] D. Peer, J. M. Karp, S. Hong, O. C. FaroKHzad, R. Margalit, R. Langer, *Nat. Nanotechnol.* **2007**, *2*, 751.

[23] C. Xu, H. Tian, H. Sun, Z. Jiao, Y. Zhang, X. Chen, *RSC Adv.* **2015**, *5*, 103380.

[24] S. Mitragotri, P. A. Burke, R. Langer, *Nat. Rev. Drug Discovery* **2014**, *13*, 655.

[25] A. N. Zelikin, C. Ehrhardt, A. M. Healy, *Nat. Chem.* **2016**, *8*, 997.

[26] A. Albanese, P. S. Tang, W. C. Chan, *Annu. Rev. Biomed. Eng.* **2012**, *14*, 1.

[27] A. C. Anselmo, S. Mitragotri, *Adv. Drug Delivery Rev.* **2017**, *108*, 51.

[28] A. Kuzmov, T. Minko, *J. Controlled Release* **2015**, *219*, 500.

[29] S. Quideau, D. Deffieux, C. Douat-Casassus, L. Pouysegu, *Angew. Chem., Int. Ed.* **2011**, *50*, 586.

[30] J. Zhou, Z. Lin, Y. Ju, M. A. Rahim, J. J. Richardson, F. Caruso, *Acc. Chem. Res.* **2020**, *53*, 1269.

[31] H. Ejima, J. J. Richardson, K. Liang, J. P. Best, M. P. van Koeverden, G. K. Such, J. Cui, F. Caruso, *Science* **2013**, *341*, 154.

[32] J. Guo, Y. Ping, H. Ejima, K. Alt, M. Meissner, J. J. Richardson, Y. Yan, K. Peter, D. von Elverfeldt, C. E. Hagemeyer, F. Caruso, *Angew. Chem., Int. Ed.* **2014**, *53*, 5546.

[33] Y. Han, Z. Lin, J. Zhou, G. Yun, R. Guo, J. J. Richardson, F. Caruso, *Angew. Chem., Int. Ed.* **2020**, *132*, 15748.

[34] J. Guo, B. L. Tardy, A. J. Christofferson, Y. Dai, J. J. Richardson, W. Zhu, M. Hu, Y. Ju, J. Cui, R. R. Dagastine, I. Yarovsky, F. Caruso, *Nat. Nanotechnol.* **2016**, *11*, 1105.

[35] G. Yun, Q. A. Besford, S. T. Johnston, J. J. Richardson, S. Pan, M. Biviano, F. Caruso, *Chem. Mater.* **2018**, *30*, 5750.

[36] M. A. Rahim, M. Bjornmalm, N. Bertleff-Zieschang, Q. Besford, S. Mettu, T. Suma, M. Faria, F. Caruso, *Adv. Mater.* **2017**, *29*, 1606717.

[37] J. Guo, X. Wang, D. C. Henstridge, J. J. Richardson, J. Cui, A. Sharma, M. A. Febbraio, K. Peter, J. B. de Haan, C. E. Hagemeyer, *Adv. Healthcare Mater.* **2015**, *4*, 2170.

[38] J. Chen, J. Li, J. Zhou, Z. Lin, F. Cavalieri, E. Czuba-Wojnilowicz, Y. Hu, A. Glab, Y. Ju, J. J. Richardson, F. Caruso, *ACS Nano* **2019**, *13*, 11653.

[39] Y. Ping, J. Guo, H. Ejima, X. Chen, J. J. Richardson, H. Sun, F. Caruso, *Small* **2015**, *11*, 2032.

[40] Y. Ju, C. Cortez-Jugo, J. Q. Chen, T. Y. Wang, A. J. Mitchell, E. Tsantikos, N. Bertleff-Zieschang, Y. W. Lin, J. Y. Song, Y. Z. Cheng, S. Mettu, M. A. Rahim, S. J. Pan, G. W. Yun, M. L. Hibbs, L. Y. Yeo, C. E. Hagemeyer, F. Caruso, *Adv. Sci.* **2020**, *7*, 1902650.

[41] Y. Ju, J. Cui, H. Sun, M. Müllner, Y. Dai, J. Guo, N. Bertleff-Zieschang, T. Suma, J. J. Richardson, F. Caruso, *Biomacromolecules* **2016**, *17*, 2268.

[42] H. Imai, N. Tochimoto, Y. Nishino, Y. Takezawa, Y. Oaki, *Cryst. Growth Des.* **2012**, *12*, 876.

[43] Y. Han, J. Zhou, Y. Hu, Z. Lin, Y. Ma, J. J. Richardson, F. Caruso, *ACS Nano* **2020**, *14*, 12972.

[44] J. Cui, Y. Yan, Y. Wang, F. Caruso, *Adv. Funct. Mater.* **2012**, *22*, 4718.

[45] D. Huesmann, A. Birke, K. Klinker, S. Türk, H. J. Räder, M. Barz, *Macromolecules* **2014**, *47*, 928.

[46] R. K. Thapa, D. B. Diep, H. H. Tønnesen, *J. Pharm. Investig.* **2021**, *51*, 377.

[47] N. Gómez-Sequeda, J. Ruiz, C. Ortiz, M. Urquiza, R. Torres, *Antibiotics* **2020**, *9*, 384.

[48] H. Gu, P. L. Ho, E. Tong, L. Wang, B. Xu, T. C. Carvalho, J. T. McConville, *Nano Lett.* **2003**, *3*, 1261.

[49] T. C. Carvalho, J. T. McConville, *J. Pharm. Pharmacol.* **2016**, *68*, 556.

[50] P. G. A. Rogueda, D. Traini, *Expert Opin. Drug Delivery* **2007**, *4*, 595.

[51] H. Sun, E. H. H. Wong, Y. Yan, J. Cui, Q. Dai, J. Guo, G. G. Qiao, F. Caruso, *Chem. Sci.* **2015**, *6*, 3505.

[52] B. R. Prasad, M. A. Brook, T. Smith, S. Zhao, Y. Chen, H. Sheardown, R. D'Souza, Y. Rochev, *Colloids Surf., B* **2010**, *78*, 237.

[53] C. D. Walkey, J. B. Olsen, H. Guo, A. Emili, W. C. Chan, *J. Am. Chem. Soc.* **2012**, *134*, 2139.

[54] K. Saha, M. Rahimi, M. Yazdani, S. T. Kim, D. F. Moyano, S. Hou, R. Das, R. Mout, F. Rezaee, M. Mahmoudi, V. M. Rotello, *ACS Nano* **2016**, *10*, 4421.

[55] W. H. Daly, D. Poché, *Tetrahedron Lett.* **1988**, *29*, 5859.

[56] M. Faria, M. Björnmalm, K. J. Thurecht, S. J. Kent, R. G. Parton, M. Kavallaris, A. P. Johnston, J. J. Gooding, S. R. Corrie, B. J. Boyd, *Nat. Nanotechnol.* **2018**, *13*, 777.

Structurally nanoengineered antimicrobial peptide polymers (SNAPPs) are promising antimicrobial agents against multidrug-resistant bacteria. Two template-assisted methods of immobilizing SNAPPs in polyphenol-based microcapsules to facilitate delivery are reported. The immobilized SNAPPs retain their antimicrobial activity as demonstrated in *E. coli*. Both capsule systems are internalized by alveolar macrophages with negligible cytotoxicity and are amenable to nebulization, demonstrating potential for pulmonary delivery.

J. Song, C. Cortez-Jugo, S. J. Shirbin, Z. Lin, S. Pan, G. G. Qiao, F. Caruso*

Immobilization and Intracellular Delivery of Structurally Nanoengineered Antimicrobial Peptide Polymers Using Polyphenol-Based Capsules